RNase 2/EDN cleaves the anticodon loops of tRNAs to produce immunostimulatory tRNA halves in asthma

Megumi Shigematsu[1], Takuya Kawamura[1], Sushrut D. Shah[2], Deepak A. Deshpande[2], and Yohei Kirino[1,*]

[1]Computational Medicine Center, [2]Center for Translational Medicine, Sidney Kimmel Medical College, Thomas Jefferson University, Philadelphia, Pennsylvania 19107, USA

*Correspondence:

Yohei Kirino, Ph.D.

1020 Locust Street, Philadelphia, PA 19107, USA

Tel: 215-503-8648

Email: Yohei.Kirino@jefferson.edu

Abstract

Asthma, the most prevalent chronic inflammatory airway disease, develops due to allergen-induced airway inflammation driven by various mediators, including proinflammatory cytokines. Our research shows that inhalation of house dust mite (HDM) in mice leads to a significant increase in the levels of tRNA half molecules in asthmatic lungs. Transcriptomic analyses of ribonucleases unequivocally identified *Ear11* (*RNase 2a/Edn*) as the most responsive endoribonuclease to HDM exposure. Indeed, human EDN is taken up by lung epithelial cells and cleaves the anticodon loops of mature tRNAs to produce tRNA halves. These tRNA halves, abundantly generated by EDN, include immunostimulatory species that promote the production of proinflammatory cytokine by activating Toll-like receptor 7. Reconstitution of the *in vitro* EDN-mediated RNA cleavage system elucidated specific positional and nucleotide preferences within the tRNA anticodon loop, providing a molecular basis for the generation of specific tRNA halves. These findings represent a previously overlooked, yet potentially critical, factor in the induction of cytokines during the pathogenesis of asthma.

Introduction

Asthma is the most prevalent chronic inflammatory disease of airways, affecting over 300 million people globally with incidence rates continuing to rise [1]. The pathogenesis of asthma encompasses allergen-induced airway inflammation, remodeling, hyperresponsiveness, and mucus hypersecretion [2-4]. These processes involve structural and functional changes in airway cells, driven by various inflammatory mediators such as cytokines, chemokines, and growth factors [5, 6]. A thorough understanding of the molecular mechanisms and regulators driving the production of these mediators is critical for unraveling the molecular pathogenesis of asthma and for the development of effective diagnostics and treatments.

We recently discovered that tRNA half molecules, the most abundant class of tRNA-derived short non-coding RNAs (sncRNAs), serve as endogenous inducers of cytokines during immune response to infection [7-9]. In human monocyte-derived macrophages (HMDMs), *Mycobacterial* infection and the accompanying activation of surface Toll-like receptors (TLRs) upregulate the NF-κB-mediated transcription of *Angiogenin (ANG)*, a tRNA cleaving endoribonuclease [10-12], inducing an accumulation of tRNA halves [7]. Among the generated 5′- and 3′-tRNA halves, the 5′-tRNA halves are selectively and abundantly packaged into the extracellular vesicles (EVs) [7, 8]. These extracellular 5′-tRNA halves are delivered into the endosomes of recipient HMDMs [7, 9], where specific species, such as those from $tRNA^{HisGUG}$ and $tRNA^{ValCAC/AAC}$ (5′-HisGUG and 5′-ValCAC/AAC), are capable of activating TLR7, leading to the production of proinflammatory cytokines [7-9]. While “foreign” single-stranded RNAs (ssRNAs) from bacteria or viruses have been extensively studied and conventionally regarded as the primary ligands for ssRNA-recognizing immune receptors like TLR7 and -8 [13, 14], the discovery of tRNA halves as abundant TLR7 stimulators has highlighted the need

to investigate “endogenous” ssRNA ligands across a variety of biological processes. However, these sncRNAs have not yet been thoroughly characterized in many diseases, including asthma.

The unexplored nature of tRNA halves could be partly attributed to the technical limitations of RNA sequencing (RNA-seq) [15, 16]. The current standard RNA-seq for sncRNAs involves ligation of 5′- and 3′-adaptors (ADs) to the 5′-monophosphate (P) and 3′-hydroxyl (OH) ends of sncRNAs, respectively. However, tRNA halves lack one or both terminal formations. 5′-tRNA halves predominantly contain a 5′-P (from mature tRNAs) and a 2′,3′-cyclic phosphate (cP), while 3′-tRNA halves possess a 5′-OH and an amino acid at the 3′-end (from mature tRNAs) [12]. These terminal formations make tRNA halves a “hidden class” of sncRNAs that standard RNA-seq fails to capture [15, 16]. A specific sequencing method designed for cP-containing RNAs (cP-RNAs), termed cP-RNA-seq [17], has been employed to characterize the expression of 5′-tRNA halves [7, 12, 18-21]. Genome-wide analyses of short cP-RNA have not only identified 5′-tRNA halves, but also 3′-tRNA halves lacking a 3′-terminal A at nucleotide position 76 (A76, according to tRNA numbering system [22]), as well as cP-RNAs derived from rRNAs and mRNAs [7, 12, 18-21].

ANG, known for its role in tRNA anticodon cleavage [7, 10-12], belongs to the RNase A superfamily. Of the 13 proteins of the RNase A superfamily encoded on the human genome, 8 have been confirmed to exhibit endoribonucleolytic activity [23, 24]. RNase 2, also known as eosinophil-derived neurotoxin (EDN), and RNase 3, known as eosinophil cationic protein (ECP), constitute major components of unique granules present in eosinophils [25]. These granulocytes function in host defense by secreting diverse inflammatory mediators [26, 27]. There are numerous reports demonstrating that the levels of EDN and ECP, along with the number of eosinophils, are elevated in the blood of asthma patients and often correlate with

disease severity [28, 29]. However, their specific molecular functions as endoribonucleases remain to be elucidated.

Although the expression of tRNA halves is induced by various biological factors, such as stress stimuli [10, 11, 20], sex hormone signaling pathways [12], and immune responses [7-9], the regulatory mechanisms governing their expression in the context of allergic reactions and inflammation in asthma remain unclear. In this study, we elucidated the expressional changes of tRNA halves induced by house dust mite (HDM) inhalation in mice, discovering a significant upregulation in asthmatic lungs. Our investigation into the ribonucleases identified EDN as the endoribonuclease taken up by lung epithelial cells, where it cleaves mature tRNAs to induce the expression of tRNA halves. Our biochemical characterization of EDN-catalyzed RNA cleavage revealed preferential positional and nucleotide patterns in the anticodon loops of tRNAs, establishing a molecular basis for EDN's production of specific immunostimulatory tRNA halves. These findings represent a potentially critical factor in the induction of cytokines involved in the molecular pathogenesis of asthma.

Results

HDM challenge significantly upregulates the expression of tRNA halves in mouse lung

To investigate the involvement of tRNA halves in asthma pathogenesis, mice were treated intranasally with HDM or PBS (as a control) for 3 weeks, followed by sncRNA characterization of their lungs. Staining of total RNAs showed an HDM-induced accumulation of sncRNAs approximately 30–40 nucleotides (nt) in length (**Fig. 1a**), which are expected to include tRNA halves and other cP-RNAs [19]. To comprehensively profile the expression of tRNA halves induced by HDM treatment, sncRNAs from the lungs of HDM-challenged mice were subjected to cP-RNA-seq [17] across three biological replicates. The lengths of the obtained tRNA-derived reads showed a bimodal distribution at 34 and 38 nt (**Fig. 1b**), typical for 5′- and 3′-tRNA halves, respectively. Indeed, among the 9 tRNA fragment (tRF) subclasses (modified from [19, 30-32]), the 5′-tRNA halves were the most abundant class of tRNA-derived sncRNAs, followed by the 3′-tRNA halves (**Fig. 1c**). The 51 tRNA isoacceptors encoded on the mouse genome did not uniformly generate 5′-tRNA halves (**Fig. 1d**). Sequence analysis of the four abundant 5′-tRNA halves has shown that cleavages generating these sncRNAs occur at specific sites within the tRNA anticodon loop (**Fig. 1e**). The primary cleavage for $tRNA^{GluCUC}$, $tRNA^{iMetCAU}$, and $tRNA^{ValCAC}$ all occurred between C and A (C36 and A37 for $tRNA^{GluCUC}$, and C34 and A35 for both $tRNA^{iMetCAU}$ and $tRNA^{ValCAC}$). The second most frequent cleavage sites for $tRNA^{GluCUC}$, $tRNA^{iMetCAU}$, and $tRNA^{ValCAC}$ were between C34 and U35, C32 and C33, and C36 and A37, respectively. For $tRNA^{HisGUG}$, cleavage predominantly occurred between U33 and G34, followed by G34 and U35. Both 5′-tRNA half species selected for TaqMan qPCR quantification were confirmed to be significantly upregulated in the lungs of HDM-treated mice

(**Fig. 1f**). Collectively, these results suggest that tRNA anticodon loops are specifically cleaved in asthmatic lungs to accumulate tRNA half molecules.

***RNase 2a/Edn* is drastically upregulated in asthmatic lungs upon HDM challenge**

We next aimed to identify the endoribonuclease responsible for the accumulation of tRNA halves by globally exploring the expressional changes of ribonucleases in the lungs of HDM-challenged mice. Utilizing a total of 49 mRNA-seq libraries from four independent studies [33-35], we conducted differential expression analyses for the 126 genes annotated as ribonucleases. The MA plot reveals a striking upregulation in the expression of *Ear11 (RNase 2a)*, corresponding to human *Edn*, in HDM-challenged mice, a pattern consistent across all four studies (**Fig. 2a**). The expression of the other ribonuclease genes either remained unchanged or showed significantly low expression, with a baseMean value of <1 (10^1).

Ear11 belongs to the *Ear* gene family, which encodes eosinophil-associated ribonucleases and is unique to rodents [36]. Unlike in humans, where 13 RNase A superfamily proteins are each encoded by a single gene [37], the mouse genome exhibits complexity (**Fig. 2b**). Due to the lack of prior literature investigating the expression profiles of *Ear* genes in mouse tissues, we individually analyzed the levels of 5 *Ears, Ear1, -2, -4, -5,* and *-11*, which are annotated as *Edn* (*RNase2, -2a, or -2b*) or *Ecp* (*Ecp1 or -2*) (**Fig. 2c**). *Ear4 (Rnase 2)* and *Ear5 (RNase 2b)* showed little expression. The expression of *Ear11 (RNase 2a)* was also negligibly low in control mice but drastically increased upon HDM challenge (**Fig. 2c**). *Ear1 (Ecp1)* exhibited modest expression, which remained unaffected by the HDM challenge. *Ear2 (Ecp1)* also showed modest expression levels, with an increase upon HDM challenge, albeit not as pronounced as observed for *Ear11*. Considering that the endoribonuclease activity of EDN is

approximately 50-fold higher than that of ECP [38, 39], together with the significantly more drastic upregulation of *Ear11 (Edn)* compared to *Ear 2 (Ecp)* upon HDM challenge, we have concluded that EDN is the primary endoribonuclease warranting further characterization in cleaving tRNAs in asthma.

EDN cleaves tRNAs to produce tRNA halves in human lung epithelial cells

Human EDN is a 134 amino acid, 15-kDa protein containing three catalytic residues: His15, Lys38, and His129 [40]. To recapitulate potential EDN-mediated tRNA cleavage in lung cells, we produced the wild-type (WT) recombinant EDN protein, as well as a mutated version in which one of the catalytic residues Lys38 was replaced with Arginine (K38R) (**Fig. 2d**). Incubation of EDN WT with HeLa total RNA led to significant degradation, while the degradation was markedly reduced with EDN K38R, demonstrating the *in vitro* ribonuclease activity of EDN WT (**Fig. 2e**). Using a classical method to quantitatively assess ribonuclease activity by measuring nucleotides in the acid-soluble fraction [41], we further confirmed the activity of EDN WT; EDN K38R showed an over 80% reduction in the activity (**Fig. 2f**).

To analyze the tRNA cleavage activity of EDN in cells, we treated A549 lung epithelial cells, as well as HeLa cells, with EDN WT. As shown in **Fig. 2g**, EDN was successfully taken up by these cells over time. TaqMan qPCR demonstrated in HeLa cells that the expression of both quantified 5′-tRNA halves, i.e., 5′-iMetCAU and 5′-HisGUG, was induced after 4 hours of treatment (**Fig. 2h**), coinciding with the cellular accumulation of EDN WT (**Fig. 2g**). Interestingly, A549 cells showed an even more pronounced EDN-mediated accumulation of the two examined 5′-tRNA halves, i.e., 5′-ValCAC and 5′-HisGUG, after 8 hours of treatment (**Fig. 2i**). This drastic accumulation of 5′-tRNA halves was observed not only within A549 cells but

also in their secreted EVs (**Fig. 2i**). Because both 5′-ValCAC and 5′-HisGUG are immunostimulatory sncRNAs capable of activating TLR7 and thus inducing proinflammatory cytokine production [7, 9], the EDN-mediated drastic accumulation of these tRNA halves in EVs from lung epithelial cells may suggest a direct link between the role of EDN-mediated tRNA cleavage and cytokine production in asthma pathogenesis.

EDN produces specific tRNA half species in human lung epithelial cells

Unlike RNase A, EDN leaves a cP at the 5′-cleavge products, such as 5′-tRNA halves, when it cleaves substrate RNAs [38], thus producing cP-RNAs. To fully elucidate the EDN-produced tRNA half species, BEAS-2B human lung epithelial cells were treated with recombinant EDN, and sncRNAs from these cells were then subjected to cP-RNA-seq. For comparison, sncRNAs from mock-treated cells were also sequenced as a control. Among the tRNA-derived reads obtained, 5′-tRNA halves appeared to be the most abundant subclass, followed by 3′-tRNA halves, in both mock- (data not shown) and EDN-treated samples (**Fig. 3a**), which is consistent with the results from HDM-treated mice (**Fig. 1c**). In the EDN-treated libraries, 5′-tRNA halves were not uniformly derived from all tRNA isoacceptors but rather from a specific subset (**Fig. 3b**). The MA plot revealed that not all abundant 5′-tRNA half species showed upregulation in relative abundance following EDN treatment. Specifically, 5′-GluCUC/UUC, 5′-ValCAC, 5′-iMetCAU, 5′-HisGUG, 5′-AspGUC, and 5′-LeuCAG were significantly upregulated, while 5′-LysCUU/UUU and 5′-GlyGCC exhibited downregulation (**Fig. 3c**). It should be noted that the fold changes shown in **Fig. 3c** are based on the comparison of the relative abundances in each library (RPM values), and therefore do not reflect changes in absolute abundances. EDN induced a drastic upregulation of 5′-tRNA haves (**Fig. 2h-i**), suggesting its potential

involvement in the production of any 5′-tRNA halves. Nonetheless, the presence of both upregulated and downregulated 5′-tRNA halves in the MA plot (**Fig. 3c**) indicates that EDN-mediated cleavage exhibits specific preferences for each tRNA species. The upregulated 5′-tRNA halves including immunostimulatory 5′-ValCAC and 5′-HisGUG, as well as 5′-iMetCAU, are expected to be preferentially generated by EDN, while the downregulated 5′-LysCUU/UUU and 5′-GlyGCC are not. Nucleotide analysis of the three upregulated 5′-tRNA halves identified the primary EDN-mediated cleavage sites in the tRNA anticodon loops between C34 and A35, and U33 and C34 (**Fig. 3d**), consistent with the cleavage patterns observed in HDM-challenged mice (**Fig. 1e**).

EDN cleaves the anticodon loops of tRNAs with specific nucleotide preferences and positional biases

To characterize the preferential cleavage patterns of EDN, we reconstituted an *in vitro* tRNA cleavage reaction using recombinant EDN. At first, endogenous tRNA fractions, gel-purified from HeLa cells, were used as substrates for the *in vitro* EDN-catalyzed cleavage. Northern blot revealed abundant production of 5′-ValCAC, 5′-HisGUG, and 5′-iMetCAU, whereas 5′-LysCUU was generated much less prominently (**Fig. 4a**). These results recapitulated the preferential EDN cleavage patterns observed in the cells (**Fig. 3c**), thus confirming that the differential expression of 5′-tRNA halves in EDN-treated cells can be attributed to EDN's preferential tRNA cleavage patterns. Furthermore, an *in vitro* EDN-catalyzed cleavage reaction using 5′-^{32}P-labeled synthetic $tRNA^{ValCAC}$ and $tRNA^{HisGUG}$ confirmed anticodon loop cleavage by EDN to generate tRNA halves (**Fig. 4b**). The large gel offering single nucleotide resolution revealed that the primary EDN cleavage of the $tRNA^{ValCAC}$ anticodon loop occurs between C34

and A35, followed by C36 and A37, while cleavage of $tRNA^{HisGUG}$ occurs between U33 and G34, followed by U35 and G36 (**Fig. 4c-d**). These results align with the cleavage sites observed in EDN-treated lung epithelial cells (**Fig. 3d**) and HDM-treated mice (**Fig. 1e**), indicating that our *in vitro* biochemical characterization accurately reflects the biological process in cells and tissues.

The cleavage patterns observed in the two tRNAs (**Fig. 4c-d**) suggest that at least C-A and U-G in anticodon loops are the preferred substrates for EDN cleavage. To further explore the substrate preferences of EDN-catalyzed anticodon loop cleavage, we utilized a variety of DNA/RNA chimeric substrates with the $tRNA^{ValCAC}$ anticodon stem-loop (ASL) sequence as a basis and a 5′-GG overhang for efficient ^{32}P labeling (**Fig. 4e**). These substrates contain only a single RNA residue at np34, with the remainder being DNA, to limit cleavage between nucleotides np34 and np35. The C34–A35 in the chimeric substate of $tRNA^{ValCAC}$ ASL (**Fig. 4e**) was efficiently cleaved by EDN WT but not by the K38R mutant (**Fig. 4f**). When we examined various combinations of nucleotides at np34 and 35 (**Fig. 4g**) for EDN-mediated cleavage activity, we found that EDN prefers to cleave after pyrimidine nucleotides C34 and U34, but it does not cleave after purine nucleotides G34 and A34 (**Fig. 4h**). This preference for cleavage after pyrimidines aligns with previous experimental results from other ribonucleases in the RNase A superfamily [42-44]. Among the eight possible combinations featuring a pyrimidine at the 5′-side (C34 and U34), the C34–A35 combination demonstrated the most efficient cleavage, followed by U34–A35 (**Fig. 4h-i**). C34–G35 and U34–G35 demonstrated less efficient but still significant cleavage, whereas the other four substrates were poor substrates for EDN cleavage (**Fig. 4h-i**). These results indicate that the presence of pyrimidines

and purines at the 5′- and 3′-sides of the cleavage sites, respectively, is crucial for efficient EDN cleavage; A outperforms G at the 5′-side, and C is more effective than U at the 3′-side.

We further analyzed preference of EDN cleavage positions within anticodon loops using DNA/RNA chimera ASL constructs that contain C–A (with C as the sole RNA to limit the cleavage between the C–A) at various positions in the anticodon loop (**Fig. 4j**). As shown in **Fig. 4k-l**, cleavage efficiency was highest between C33–A34, followed by C32–A33, C34–A35, and C35–A36. Interestingly, efficiency decreased for sites located on the 3′-side of the anticodon loop, such as between C36–A37 and C37–A38 (**Fig. 4k-l**). To analyze universality of these positional biases, we further examined the ASL constructs containing G–U at various positions in the anticodon loop (**Fig. 4m**), yielding identical preference patterns (**Fig. 4n-o**). These results suggest that EDN recognizes and prefers the 5′-side of anticodon loop for cleavage. Together with its nucleotide preferences, these defined cleavage patterns by EDN explain why specific 5′-tRNA halves are preferentially generated by EDN in asthma.

Discussion

Eosinophils are associated with various pathological conditions and exhibit elevated levels in a range of diseases, including asthma, parasitic infections, and certain autoimmune diseases [45, 46]. These cells migrate to sites of inflammation or infection, where they contribute to the inflammatory response by releasing cytokines, growth factors, and proteins stored in eosinophilic granules, such as EDN [25-27]. In asthma, eosinophils are recruited to the airways during inflammatory conditions [47-49]. In a murine model of asthma, we identified *Ear11* (*Rnase 2a/Edn*), an eosinophil-associated ribonuclease, as the most responsive ribonuclease to HDM challenge, explaining the observed robust upregulation of tRNA halves in the lungs of HDM-challenged mice. Indeed, our analyses further demonstrated that human EDN catalyzes the cleavage of the anticodon loop of mature tRNAs to produce tRNA halves both *in vitro* and in lung epithelial cells, suggesting that EDN released from eosinophils abundantly generate tRNA halves in airway cells during asthma pathogenesis.

The RNase A superfamily is the best studied ribonuclease family in biochemistry and serves as the primary model for understanding acid-base catalysts [50]. Despite this, the endogenous substrates of these ribonucleases, the consequences of substrate cleavages, and their regulation in the context of diseases remain poorly investigated. It is well-known that the levels of EDN increase in the blood of asthma patients [28, 29] and that EDN exhibits cytotoxic effects in lung epithelial cells [48, 49], yet few studies have explored these associations further. Our cP-RNA-seq identified HDM-induced tRNA halves in mouse lungs and EDN-generated tRNA halves in human lung epithelial cells. Notably, the cP-RNA transcriptome in mice reflects the consequences of asthmatic condition established by HDM-challenge over three weeks, resulting from multiple layers of processes including not only EDN-catalyzed tRNA cleavage

but also potential constitutive cleavages by other ribonucleases and the balance between stabilization and degradation over a relatively long period. In contrast, the cP-RNA transcriptome in human epithelial cells, resulting from acute exposure to EDN, predominantly reflects EDN-generated tRNA halves.

We discovered that several 5′-tRNA halves, including 5′-HisGUG, 5′-ValCAC, and 5′-iMetCAU, are preferentially produced by EDN, while others, such as 5′-LysCUU/UUU and 5′-GlyGCC, are not. Our biochemical characterization using an *in vitro* EDN cleavage system revealed specific nucleotide preferences and positional biases in the anticodon loops targeted by EDN. EDN exhibited a strong cleavage preference toward C–A, followed by U–A, C–G, and U–G, with cleavage occurring preferentially on the 5′-side of the anticodon loop. These results provide a molecular basis for why specific tRNAs are preferred targets of EDN, such as $tRNA^{HisGUG}$, $tRNA^{ValCAC}$, $tRNA^{iMetCAU}$, $tRNA^{AspGUC}$, and $tRNA^{LeuCAG}$, all of which have CA, UA, or UG sequences on the 5′-side of anticodon loop. This elucidates the molecular mechanisms shaping the profiles of EDN-generated tRNA halves.

Among the specific tRNA half species generated by EDN, two species, 5′-HisGUG and 5′-ValCAC, possess immunostimulatory activities that can induce the production of proinflammatory cytokines through the stimulation of TLR7 [7-9]. Given that our study has experimentally demonstrated the EDN-induced accumulation of these immunostimulatory tRNA halves not only in airway epithelial cells but also their secreted EVs, we propose that these extracellular tRNA halves, generated by EDN and secreted from airway cells, could be delivered to the endosomes of surrounding airway cells and immune cells, activating TLR7 and thus functioning as novel mediators that contribute significantly to elevated levels of proinflammatory cytokines in asthma. The immunostimulatory roles of EDN-produced tRNA

halves may also be involved in the pathobiology of other diseases associated with elevated eosinophils levels. The expression levels and/or profiles of extracellular tRNA halves could serve as noninvasive biomarkers indicative of the severity of inflammation and infection. Given the reported variety of molecular functions of tRNA halves beyond immune receptor activation, including the regulation of gene expression and translation in the cytoplasm [15, 16], it is possible that EDN-generated tRNA halves could also play various key cytoplasmic roles in the molecular pathogenesis of asthma.

Materials and Methods

Ethics statement

All mouse experiments complied with the National Institutes of Health (NIH) standards and guidelines and received approval from the Institutional Animal Care and Use Committee at Thomas Jefferson University (TJU).

Mouse models of allergic asthma

Intranasal challenges with HDM were performed as described previously [51]. Briefly, 8-week-old female C57BL/6 mice received intranasal challenges with 25 μg of HDM extract (Dermatophagoides pteronyssinus, Greer Labs) in 35 μl saline, 5 days a week for 3 consecutive weeks. Lungs were harvested for analysis 24 h after the final challenge.

Human cell lines and EDN treatment

HeLa, A549, and BEAS-2B cells were originally sourced from ATCC (CCL-2, CCL-185, and CRL-3588, respectively). HeLa and A549 cells were cultured in DMEM containing 10% FBS, while BEAS-2B cells were cultured in DMEM/F12 also supplemented with 10% FBS. These cells were treated with recombinant EDN at a concentration of 2 μg/ml.

RNA isolation and northern blot

Total RNA was extracted from frozen tissues using TRIsure (Bioline) as previously described [19]. Total RNA from culture cells was also extracted using TRIsure, following the manufacturer's instructions. Northern blot was performed as previously described [7, 20, 21] using the following antisense probes: 5′-ValCAC, 5′- GAGGCGAACGTGATAACCACTA-3′;

5′-HisGUG, 5′-GCAGAGTACTAACCACTATACG-3′; 5′-iMetCAU, 5′-GCTTCCGCTGCGCCACTCT-3′; and 5′-LysCUU, 5′- GTCTCATGCTCTACCGACTG-3′.

cP-RNA-seq and bioinformatics

Short RNAs ranging from 20 to 50 nt were gel-purified from the total RNA extracted from mouse lungs and then subjected to the cP-RNA-seq procedure as previously described [7, 12, 17-21]. The resulting amplified cDNAs were gel-purified and sequenced using the Illumina NextSeq 500 at the MetaOmics Core Facility of the Sidney Kimmel Cancer Center (SKCC) at TJU. The cP-RNA-seq libraries generated approximately 26–34 million raw reads and have been deposited in the NCBI Sequence Read Archive under accession number PRJNA525110 (**Supplementary Table S1**). The cP-RNA-seq analysis of BEAS-2B cells was performed using short RNAs isolated with the mirVana miRNA Isolation Kit (Thermo Fisher Scientific). The cP-RNA-seq libraries produced ~2–10 million raw reads and have been deposited in the NCBI Sequence Read Archive under PRJNA1099176 (**Supplementary Table S1**).

Bioinformatics analyses were conducted following previously described procedures [19, 20]. Briefly, reads were quality filtered and those between 20-50-nt were extracted using Cutadapt (doi.org/10.14806/ej.17.1.200). These filtered reads were then mapped to cytoplasmic mature tRNAs, rRNAs, mRNAs, mitochondrial transcripts, and the whole genome. The reference tRNA sequences were obtained from the Genomic tRNA database [52], and the GRCm38/mm10 and GRCh37/hg19 of Release 18 were used for mouse and human, respectively. For expression and sequence analyses and for data visualization, we utilized FastQC, along with several R packages including DESeq2 [53], ggplot2, and gplots.

For the analysis of mRNA expression of RNase A-type endoribonucleases, we selected four independent projects: PRJNA212775 [33], PRJNA547063 [34], PRJNA522698 [34], and PRJNA480707 [35]. The STAR aligner [54] was employed to map the reads to mouse transcripts. The phylogenetic tree was created using MEGA11 [55].

Quantification of RNAs by TaqMan qPCR and standard qPCR

5′-tRNA halves were specifically quantified using TaqMan qPCR as described previously [7, 12, 19, 21]. Briefly, to remove cP from 5′-tRNA halves, total RNA was treated with T4 polynucleotide kinase (New England Biolabs), followed by ligation to a 3′-RNA adaptor using T4 RNA ligase (Thermo Fisher Scientific). The ligated RNA was then subjected to TaqMan qPCR using the One Step PrimeScript RT-PCR Kit (Takara Bio), with 200 nM of a TaqMan probe targeting the boundary of the target RNA and the 3′-AD, along with forward and reverse primers. ActB mRNA was quantified by standard qPCR. Briefly, total RNA was treated with DNase I (Promega) and subjected to reverse transcription using RevertAid Reverse Transcriptase (Thermo Fisher Scientific) and a reverse primer. The synthesized cDNAs were then subjected to PCR using 2×qPCR Master Mix (Bioland) with forward and reverse primers. The sequences of the 3′-RNA adaptor, TaqMan probes, and primers are shown in **Supplementary Table S2**.

Recombinant EDN and its ribonucleolytic activity

The coding region of the human *RNase 2 (Edn)* gene was cloned into pET-21a plasmid, enabling the expression of a C-terminal 6× His-tagged EDN protein. A plasmid encoding the K38R mutant *Edn* was produced through site-directed mutagenesis. The wild-type or K38R

mutant EDN was expressed in *E. coli* BL21 (DE3) pLysS as described previously [56]. After harvesting, the cells were suspended in lysis buffer containing 50 mM Tris-HCl pH8.0, 2 mM EDTA, 0.5% Triton-X100, 10% glycerol, and 0.7 mg/ml lysozyme. After sonication, the insoluble fraction, which contained recombinant EDN, was denatured and subsequently refolded in the presence of oxidized glutathione as described previously [57]. The refolded protein fraction underwent overnight dialysis against IEX buffer A, consisting of 20 mM Tris-HCl pH7.5, 0.2% Triton X-100, and 2% glycerol. The supernatant from the dialyzed solution was then applied to a HiTrap SP HP column (Cytiva) for the purification of His-tagged EDN. The purified protein was stored in a buffer containing 10 mM Tris-HCl pH7.5, 50 mM NaCl, 4 mM DTT, and 40% glycerol. The ribonucleolytic activity of the purified EDN was assessed using the Kunitz assay that measures the release of nucleotides into the acid soluble fraction [58].

Western blot

Western blot was performed as described previously [7, 21]. The primary antibodies used were anti-His6-tag monoclonal antibody (6*His, Proteintech) and anti-GAPDH monoclonal antibody (Proteintech).

EV isolation

EVs were isolated from the culture medium of A549 cells according to an ultracentrifugation-based method described previously [7, 9]. Successful EV isolation was verified by western blot, nanoparticle tracking analysis, and transmission electron microscopy, as in our previous study [7].

In vitro RNA synthesis

The synthetic $tRNA^{ValCAC}$ and $tRNA^{HisGUG}$ were synthesized by an *in vitro* RNA transcription reaction as described previously [7, 21, 59]. dsDNA templates were generated using T7 DNA Polymerase (New England Biolabs) and then subjected to an *in vitro* transcription reaction with T7 RNA polymerase (New England Biolabs) at 37°C for 6 h. The synthesized RNAs were gel-purified using denaturing PAGE with single nucleotide resolution. DNA/RNA chimeras were synthesized by integrated DNA Technologies. The sequences of the synthetic RNAs are shown in **Supplementary Table S3**.

In vitro RNA cleavage assay

Substrate tRNAs or DNA/RNA chimera ASLs were ^{32}P-labeled at their 5′-end, and a trace amount of these labeled RNAs was mixed with unlabeled RNAs. The substrates were then incubated with recombinant EDN. For the biochemical characterization of EDN, a buffer containing 50 mM MES pH6.0, 25 mM NaCl, and 0.1 mg/mL BSA was used, unless otherwise indicated. The reaction mixtures also included $MgCl_2$; 20 mM for synthetic tRNAs and 10 mM for ASLs. After incubation at 37°C, the cleaved products were resolved on denaturing PAGE. For the cleavage assay using the native tRNA fraction, 500 ng of gel-purified tRNA fractions from HeLa cells were incubated with 0, 1, 5, or 25 nM of EDN for 1 min in a buffer containing 50 mM MES pH5.5, 20 mM $MgCl_2$, and 0.1 mg/ml BSA. The ^{32}P-labeled RNA signal was detected using a phosphor imager. Image analysis was performed with ImageJ [60].

Acknowledgements

We are grateful to the members of our laboratories for helpful discussions. This study was supported by the National Institutes of Health Grant (AI130496 to DD and YK, GM106047 to YK, and HL137030 to DD), American Cancer Society Research Scholar Grant (RSG-17-059-01-RMC, to YK), W.W. Smith Charitable Trust Grant (C1608, to YK), Japan Society for the Promotion of Science Postdoctoral Fellowship for Research Abroad (to MS), and American Lung Association Catalyst Award Grant (to MS). The authors declare no competing financial interests.

References

1. Holgate, S.T., et al., *Asthma.* Nat Rev Dis Primers, 2015. **1**(1): p. 15025.
2. Hough, K.P., et al., *Airway Remodeling in Asthma.* Front Med (Lausanne), 2020. **7**: p. 191.
3. Fehrenbach, H., C. Wagner, and M. Wegmann, *Airway remodeling in asthma: what really matters.* Cell Tissue Res, 2017. **367**(3): p. 551-569.
4. Bergeron, C., W. Al-Ramli, and Q. Hamid, *Remodeling in asthma.* Proc Am Thorac Soc, 2009. **6**(3): p. 301-5.
5. Lambrecht, B.N., H. Hammad, and J.V. Fahy, *The Cytokines of Asthma.* Immunity, 2019. **50**(4): p. 975-991.
6. Chung, K.F. and P.J. Barnes, *Cytokines in asthma.* Thorax, 1999. **54**(9): p. 825-57.
7. Pawar, K., et al., *Infection-induced 5'-half molecules of tRNAHisGUG activate Toll-like receptor 7.* PLoS Biol, 2020. **18**(12): p. e3000982.
8. Gumas, J., et al., *Immunostimulatory short non-coding RNAs in the circulation of patients with tuberculosis infection.* Mol Ther Nucleic Acids, 2024. **35**(1): p. 102156.
9. Pawar, K., T. Kawamura, and Y. Kirino, *The tRNA(Val) half: A strong endogenous Toll-like receptor 7 ligand with a 5'-terminal universal sequence signature.* Proc Natl Acad Sci U S A, 2024. **121**(19): p. e2319569121.
10. Yamasaki, S., et al., *Angiogenin cleaves tRNA and promotes stress-induced translational repression.* J Cell Biol, 2009. **185**(1): p. 35-42.
11. Fu, H., et al., *Stress induces tRNA cleavage by angiogenin in mammalian cells.* FEBS Lett, 2009. **583**(2): p. 437-42.
12. Honda, S., et al., *Sex hormone-dependent tRNA halves enhance cell proliferation in breast and prostate cancers.* Proc Natl Acad Sci U S A, 2015. **112**(29): p. E3816-25.
13. Heil, F., et al., *Species-specific recognition of single-stranded RNA via toll-like receptor 7 and 8.* Science, 2004. **303**(5663): p. 1526-9.
14. Melchjorsen, J., et al., *Activation of innate defense against a paramyxovirus is mediated by RIG-I and TLR7 and TLR8 in a cell-type-specific manner.* J Virol, 2005. **79**(20): p. 12944-51.
15. Shigematsu, M., T. Kawamura, and Y. Kirino, *Generation of 2',3'-Cyclic Phosphate-Containing RNAs as a Hidden Layer of the Transcriptome.* Front Genet, 2018. **9**: p. 562.
16. Shigematsu, M. and Y. Kirino, *Making Invisible RNA Visible: Discriminative Sequencing Methods for RNA Molecules with Specific Terminal Formations.* Biomolecules, 2022. **12**(5).
17. Honda, S., K. Morichika, and Y. Kirino, *Selective amplification and sequencing of cyclic phosphate-containing RNAs by the cP-RNA-seq method.* Nat Protoc, 2016. **11**(3): p. 476-89.
18. Honda, S., et al., *The biogenesis pathway of tRNA-derived piRNAs in Bombyx germ cells.* Nucleic Acids Res, 2017. **45**(15): p. 9108-9120.
19. Shigematsu, M., et al., *Genome-wide identification of short 2',3'-cyclic phosphate-containing RNAs and their regulation in aging.* PLoS Genet, 2019. **15**(11): p. e1008469.
20. Shigematsu, M. and Y. Kirino, *Oxidative stress enhances the expression of 2',3'-cyclic phosphate-containing RNAs.* RNA Biol, 2020. **17**(8): p. 1060-1069.

21. Shigematsu, M., et al., *RNase kappa promotes robust piRNA production by generating 2',3'-cyclic phosphate-containing precursors.* Nat Commun, 2021. **12**(1): p. 4498.
22. Sprinzl, M. and K.S. Vassilenko, *Compilation of tRNA sequences and sequences of tRNA genes.* Nucleic Acids Res, 2005. **33**(Database issue): p. D139-40.
23. Dyer, K.D. and H.F. Rosenberg, *The RNase a superfamily: generation of diversity and innate host defense.* Mol Divers, 2006. **10**(4): p. 585-97.
24. Sorrentino, S., *The eight human "canonical" ribonucleases: molecular diversity, catalytic properties, and special biological actions of the enzyme proteins.* FEBS Lett, 2010. **584**(11): p. 2194-200.
25. Acharya, K.R. and S.J. Ackerman, *Eosinophil granule proteins: form and function.* J Biol Chem, 2014. **289**(25): p. 17406-15.
26. McBrien, C.N. and A. Menzies-Gow, *The Biology of Eosinophils and Their Role in Asthma.* Front Med (Lausanne), 2017. **4**: p. 93.
27. Thomas, L.H. and J.A. Warner, *The eosinophil and its role in asthma.* Gen Pharmacol, 1996. **27**(4): p. 593-7.
28. Venge, P., *Monitoring the allergic inflammation.* Allergy, 2004. **59**(1): p. 26-32.
29. Malinovschi, A., et al., *Clinical Potential of Eosinophil-Derived Neurotoxin in Asthma Management.* J Allergy Clin Immunol Pract, 2023. **11**(3): p. 750-761.
30. Lee, Y.S., et al., *A novel class of small RNAs: tRNA-derived RNA fragments (tRFs).* Genes Dev, 2009. **23**(22): p. 2639-49.
31. Wilson, B. and A. Dutta, *Function and Therapeutic Implications of tRNA Derived Small RNAs.* Front Mol Biosci, 2022. **9**: p. 888424.
32. Magee, R. and I. Rigoutsos, *On the expanding roles of tRNA fragments in modulating cell behavior.* Nucleic Acids Res, 2020. **48**(17): p. 9433-9448.
33. Kinker, K.G., et al., *Overexpression of dimethylarginine dimethylaminohydrolase 1 attenuates airway inflammation in a mouse model of asthma.* PLoS One, 2014. **9**(1): p. e85148.
34. Ramelli, S.C., et al., *Nanoparticle Delivery of Anti-inflammatory LNA Oligonucleotides Prevents Airway Inflammation in a HDM Model of Asthma.* Mol Ther Nucleic Acids, 2020. **19**: p. 1000-1014.
35. Pascoe, C.D., et al., *The importance of reporting house dust mite endotoxin abundance: impact on the lung transcriptome.* Am J Physiol Lung Cell Mol Physiol, 2020. **318**(6): p. L1229-L1236.
36. Zhang, J., K.D. Dyer, and H.F. Rosenberg, *Evolution of the rodent eosinophil-associated RNase gene family by rapid gene sorting and positive selection.* Proc Natl Acad Sci U S A, 2000. **97**(9): p. 4701-6.
37. Cho, S. and J. Zhang, *Ancient expansion of the ribonuclease A superfamily revealed by genomic analysis of placental and marsupial mammals.* Gene, 2006. **373**: p. 116-25.
38. Sorrentino, S., et al., *Eosinophil-derived neurotoxin and human liver ribonuclease. Identity of structure and linkage of neurotoxicity to nuclease activity.* J Biol Chem, 1992. **267**(21): p. 14859-65.
39. Sorrentino, S. and D.G. Glitz, *Ribonuclease activity and substrate preference of human eosinophil cationic protein (ECP).* FEBS Lett, 1991. **288**(1-2): p. 23-6.

40. Rosenberg, H.F. and K.D. Dyer, *Eosinophil cationic protein and eosinophil-derived neurotoxin. Evolution of novel function in a primate ribonuclease gene family.* J Biol Chem, 1995. **270**(50): p. 30234.
41. Isobe, K. and S. Uchiyama, *An assay for ribonuclease activity, based on ultraviolet absorption of RNA hydrolysate, using phosphotungstic acid.* J Biochem Biophys Methods, 1986. **12**(5-6): p. 299-303.
42. Borkakoti, N., *Enzyme specificity: base recognition and hydrolysis of RNA by ribonuclease A.* FEBS Lett, 1983. **162**(2): p. 367-73.
43. Kelemen, B.R., et al., *Excavating an active site: the nucleobase specificity of ribonuclease A.* Biochemistry, 2000. **39**(47): p. 14487-94.
44. Rybak, S.M. and B.L. Vallee, *Base cleavage specificity of angiogenin with Saccharomyces cerevisiae and Escherichia coli 5S RNAs.* Biochemistry, 1988. **27**(7): p. 2288-94.
45. Rosenberg, H.F., K.D. Dyer, and P.S. Foster, *Eosinophils: changing perspectives in health and disease.* Nat Rev Immunol, 2013. **13**(1): p. 9-22.
46. Jackson, D.J., P. Akuthota, and F. Roufosse, *Eosinophils and eosinophilic immune dysfunction in health and disease.* Eur Respir Rev, 2022. **31**(163).
47. Trivedi, S.G. and C.M. Lloyd, *Eosinophils in the pathogenesis of allergic airways disease.* Cell Mol Life Sci, 2007. **64**(10): p. 1269-89.
48. Venge, P., et al., *Epithelial injury by human eosinophils.* Am Rev Respir Dis, 1988. **138**(6 Pt 2): p. S54-7.
49. Gleich, G.J., et al., *The eosinophil as a mediator of damage to respiratory epithelium: a model for bronchial hyperreactivity.* J Allergy Clin Immunol, 1988. **81**(5 Pt 1): p. 776-81.
50. Thompson, J.E. and R.T. Raines, *Value of general Acid-base catalysis to ribonuclease a.* J Am Chem Soc, 1994. **116**(12): p. 5467-8.
51. Sharma, P., et al., *Bitter Taste Receptor Agonists Mitigate Features of Allergic Asthma in Mice.* Sci Rep, 2017. **7**: p. 46166.
52. Chan, P.P. and T.M. Lowe, *GtRNAdb 2.0: an expanded database of transfer RNA genes identified in complete and draft genomes.* Nucleic Acids Res, 2016. **44**(D1): p. D184-9.
53. Love, M.I., W. Huber, and S. Anders, *Moderated estimation of fold change and dispersion for RNA-seq data with DESeq2.* Genome Biol, 2014. **15**(12): p. 550.
54. Dobin, A., et al., *STAR: ultrafast universal RNA-seq aligner.* Bioinformatics, 2013. **29**(1): p. 15-21.
55. Tamura, K., G. Stecher, and S. Kumar, *MEGA11: Molecular Evolutionary Genetics Analysis Version 11.* Mol Biol Evol, 2021. **38**(7): p. 3022-3027.
56. Boix, E., *Eosinophil cationic protein.* Methods Enzymol, 2001. **341**: p. 287-305.
57. Newton, D.L., et al., *Angiogenin single-chain immunofusions: influence of peptide linkers and spacers between fusion protein domains.* Biochemistry, 1996. **35**(2): p. 545-53.
58. Wu, Y., H. Wang, and T. Ng, *Purification and characterization of a novel RNase with antiproliferative activity from the mushroom Lactarius flavidulus.* J Antibiot (Tokyo), 2012. **65**(2): p. 67-72.
59. Shigematsu, M. and Y. Kirino, *5'-Terminal nucleotide variations in human cytoplasmic tRNAHisGUG and its 5'-halves.* RNA, 2017. **23**(2): p. 161-168.

60. Schneider, C.A., W.S. Rasband, and K.W. Eliceiri, *NIH Image to ImageJ: 25 years of image analysis.* Nat Methods, 2012. **9**(7): p. 671-5.

Figure legends

Figure 1. Characterization of 5′-tRNA halves in the lungs of HDM-challenged mice

(a) Total lung RNAs were developed using denaturing PAGE and stained with SYBR Gold. The regions containing sncRNAs that accumulated in the lungs of HDM-challenged mice are indicated by a blue line.

(b) Length distribution of tRNA-mapped reads. The shaded region represents the standard deviation (SD) across three replicates.

(c) tRNA-mapped reads were classified into nine distinct types of tRFs. Briefly, 5′- and 3′-halves retain the intact 5′- and 3′-ends of mature tRNAs, respectively, and are generated by cleavage within the anticodon loop. 5′- and 3′-tRFs also retain the mature tRNA ends but are cleaved outside the anticodon loop; they either exclude the anticodon loop (short, S) or include it (long, L). i-tRFs are derived from internal tRNA regions and lack any mature ends. Among them, i-tRF-5′ and i-tRF-3′ are derived from the 5′- and 3′-halves, respectively, while i-tRFs encompassing the anticodon loop are referred to as i-tRF-AL. Error bars indicate the SD from three replicates.

(d) The abundance of 5′-tRNA halves is visualized in a heatmap.

(e) Cloverleaf structures of selected tRNAs. The 5′-tRNA halves are highlighted in blue. The primary cleavage positions within the anticodon loops are also indicated in blue, whereas the second most abundant cleavage positions are shown in light blue. SDs are shown for three replicates.

(f) TaqMan qPCR was performed to quantify 5′-tRNA halves, with the results normalized to U6 snRNA levels. The levels of ActB mRNA were quantified using standard qPCR and also

normalized to U6 snRNA levels. Sample number: n=6 for each cohort (one of the saline samples for 5′-ValCAC was not detected). Students' t-test: **p<0.01; ***p<0.001.

Figure 2. Activity of EDN in human lung epithelial cells

(a) The MA plot of mouse ribonucleases shows the differential expression in the lungs of HDM-challenged mice compared to control mice. The y-axis represents fold changes, while the x-axis indicates the mean value of each read. Datasets are derived from four independent studies: (i) PRJNA212775 [33]; (ii) PRJNA547063 [34]; (iii) PRJNA522698 [34]; and (iv) PRJNA480707 [35].

(b) Phylogenetic tree of murine genes of RNase A superfamily.

(c) The mRNA expression levels of 5 *Ears*, annotated as *Edn* or *Ecp*, are shown as RPKM. IL-13 serves as a positive control for HDM treatment. The color codes align with (**a**). PRJNA480707 employed two doses of HDM, with green squares and circles indicating low and high doses, respectively.

(d) Recombinant human EDN WT and the K38R mutant.

(e) Ribonuclease activity of EDN and RNase A was assessed by cleaving HeLa total RNA. The cleaved RNAs were developed using denaturing PAGE and stained with SYBR Gold.

(f) Kunits assay performed to quantitatively assess the activity of EDN. Three independent assays were performed, and the error bars indicate the SD.

(g) HeLa and A549 cells were treated with EDN and harvested by trypsinization to remove excess EDN from the cell surfaces. The uptake of EDN was detected by western blot targeting the histidine tag.

(h, i) Total RNAs extracted from EDN-treated HeLa cells (h) and from EDN-treated A549 cells and their EVs (i) were subjected to TaqMan qPCR for the specific quantification of 5′-tRNA halves, with the results from the cells normalized to 5S rRNA levels. The error bars indicate the SD from three technical replicates of the qPCR (f) and from three biological replicates (g).

Figure 3. Characterization of EDN-generated 5′-tRNA halves

(a) tRNA-mapped reads from EDN-treated BEAS-2B cells were classified into nine distinct types of tRFs. Error bars indicate the SD from three biological replicates.

(b) The abundance of EDN-produced 5′-tRNA halves is visualized in a heatmap.

(c) The MA plot of 5′-tRNA halves shows the differential expression in EDN-treated BEAS-2B cells compared to mock treatment. The y-axis represents fold changes, while the x-axis indicates the mean value of each read. The abundant 5′-tRNA halves are individually labeled.

(d) Analyses of the 3′-terminal nucleotides of the selected three abundant 5′-tRNA halves in EDN-treated BEAS-2B cells.

Figure 4. Nucleotide and positional preferences in EDN-mediated anticodon loop cleavage

(a) Total tRNA fractions from HeLa cells were subjected to *in vitro* cleavage catalyzed by EDN, and the generated 5′-tRNA halves were detected using northern blots. The reaction was performed in an assay buffer of pH5.5.

(b) 250 nM of synthetic $tRNA^{ValCAC}$ and $tRNA^{HisGUG}$ were incubated with 0.5 nM of EDN for 15, 30, 60, and 90 sec. The EDN-mediated cleavages and resultant generation of 5′-tRNA halves were detected by the ^{32}P signals on denaturing PAGE.

(c) The reactions from (b) were subjected to analytical denaturing PAGE, which enables substrate separation at a single nucleotide level. Al: alkaline ladder, indicating single nucleotide differences; T1: a ladder obtained by RNase T1 digestion that cleaves at the 3′-end of guanosine. Two primary cleavage sites within the anticodon loops are highlighted.

(d) Cloverleaf structures of $tRNA^{ValCAC}$ and $tRNA^{HisGUG}$, with their EDN cleavage sites within the anticodon loops indicated.

(e, g, j, m) Structures of the ASL substrates. These substrates contain only one RNA residue, as indicated by rN, with the remainder being DNA.

(f, h, k, n) 250 nM of ASL substrates were incubated with 0.5 nM of EDN for 10, 30, and 60 sec (f) or for 30 sec (h, k, and n). The products of EDN-mediated cleavages were detected by the ^{32}P signals on denaturing PAGE.

(i) The EDN-mediated cleavage rate for each ASL substrate in (h) was quantified. The error bars indicate SD from three independent experiments.

(l, o) In experiment (k) or (n), the relative cleavage efficiency compared to C34 or G34 substrate is shown. Error bars denote the SDs obtained from three independent experiments.

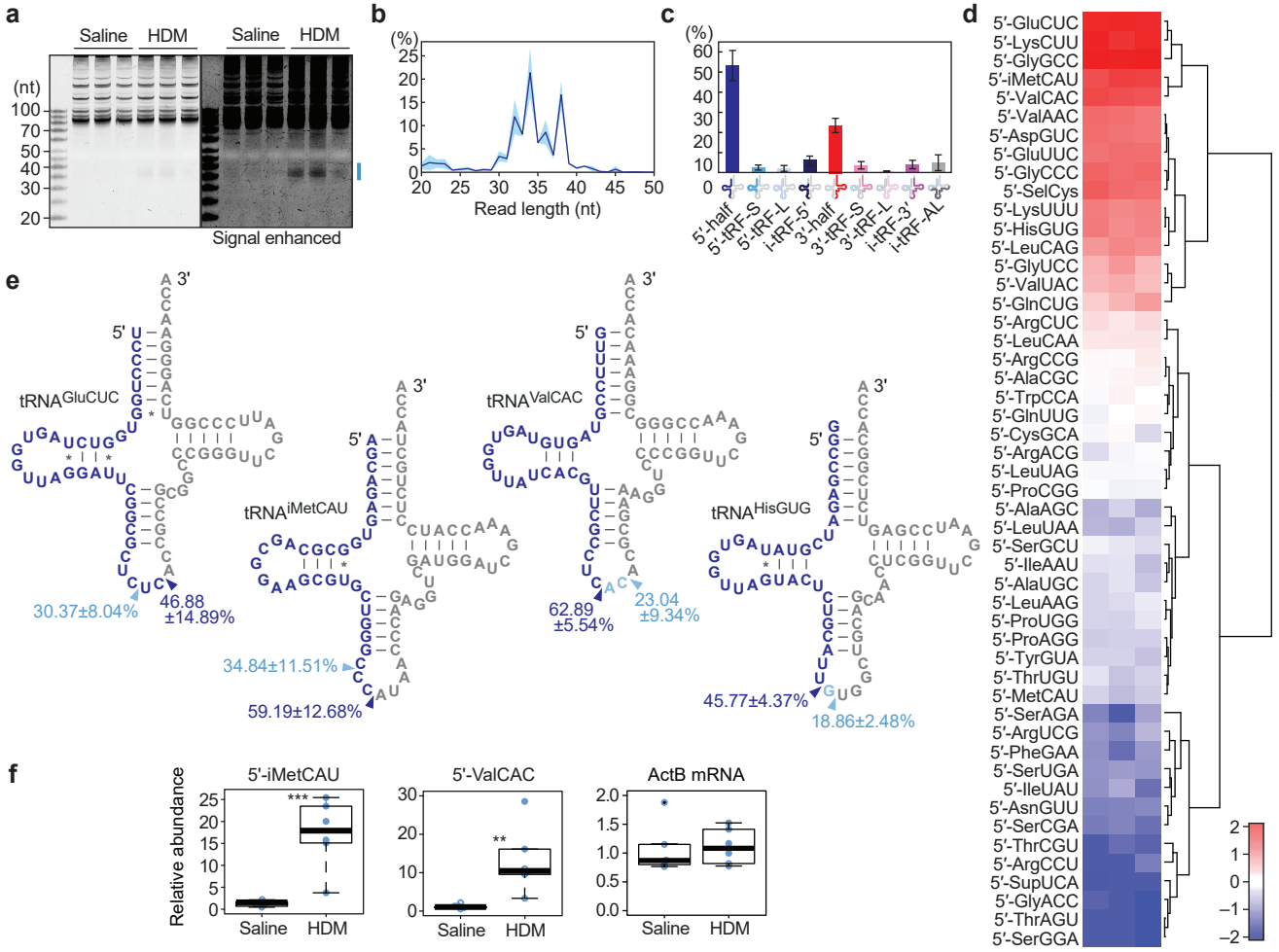

Shigematsu et al. Figure 1

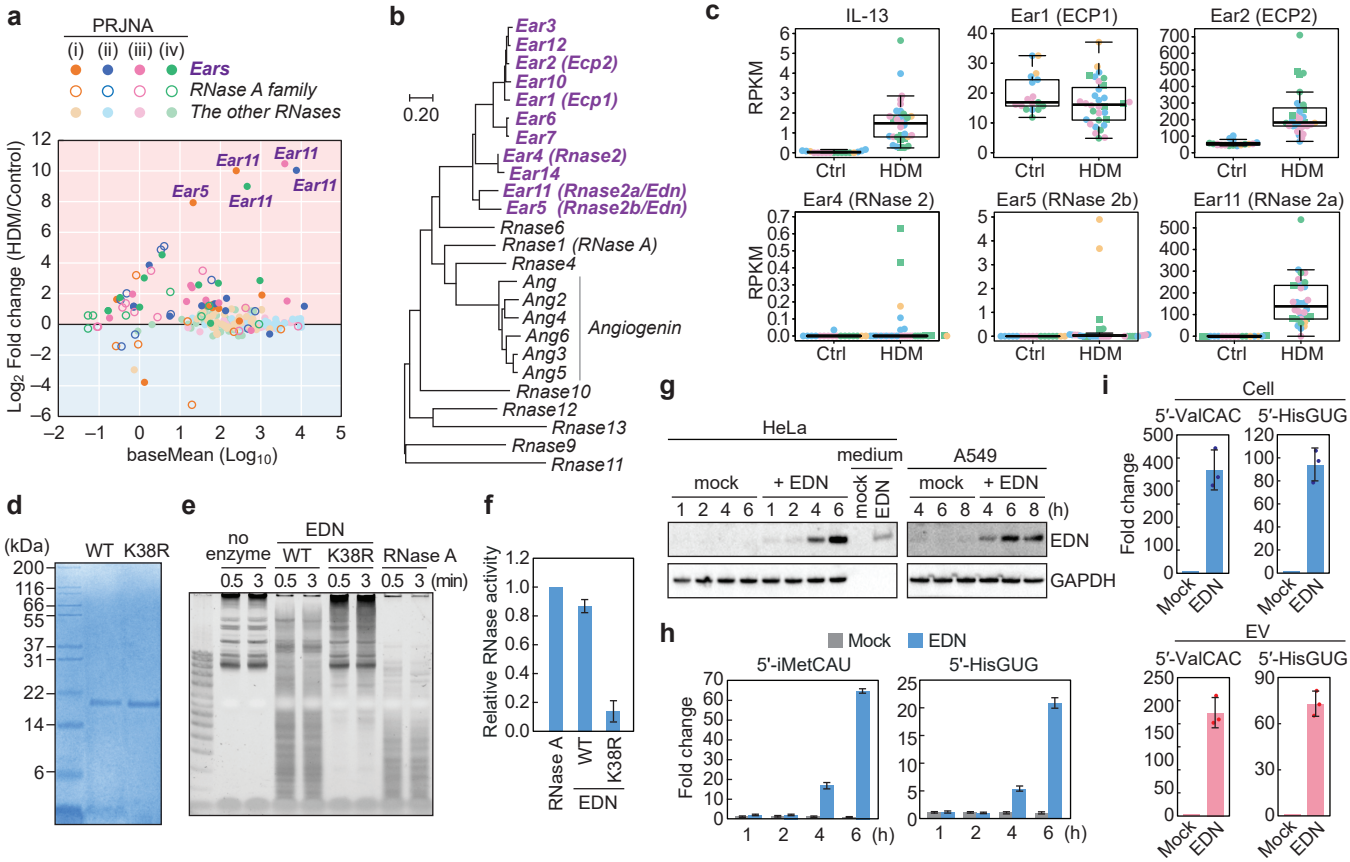

Shigematsu et al. Figure 2

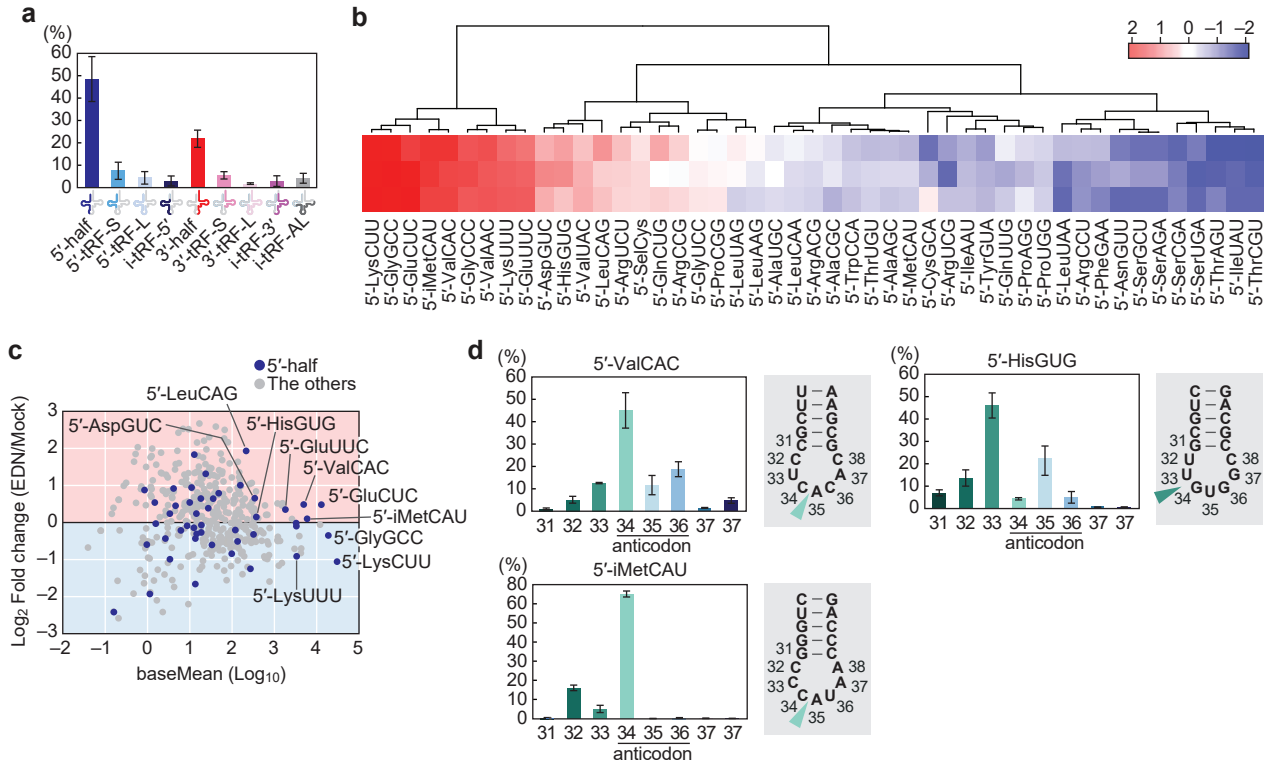

Shigematsu et al. Figure 3

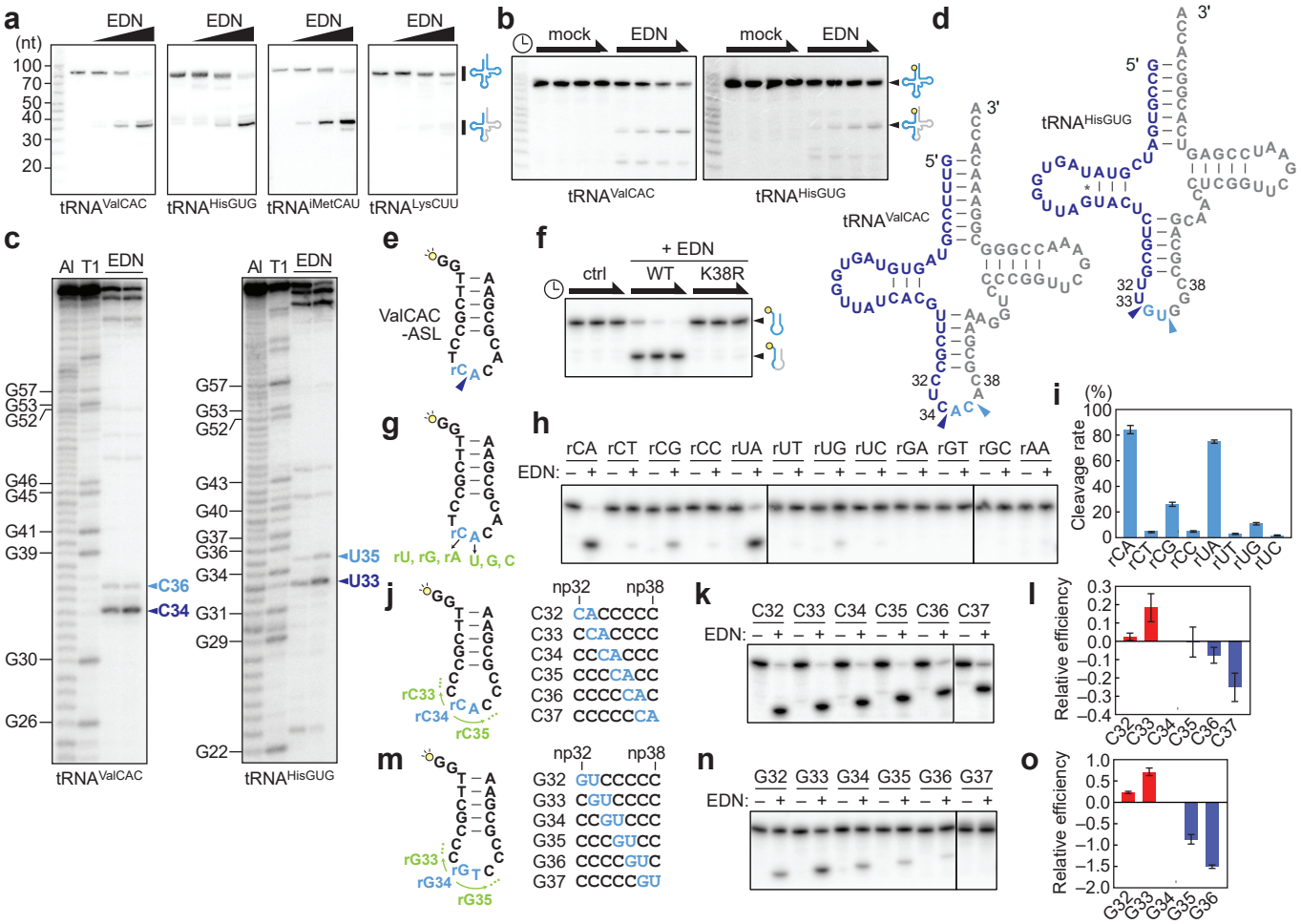

Shigematsu et al. Figure 4